12-1-2018

Automated quantification and evaluation of motion artifact on coronary CT angiography images

Hongfeng Ma
Marquette University

Eric Gros
GE Healthcare

Scott G. Baginski
Medical College of Wisconsin

Zachary R. Laste
Medical College of Wisconsin

Naveen M. Kulkarni
Medical College of Wisconsin

See next page for additional authors

Medical Physics, Vol. 45, No. 12 (December 2018): 5494-5508. DOI.

Automated quantification and evaluation of motion artifact on coronary CT angiography images

Hongfeng Ma
Department of Biomedical Engineering, Marquette University and Medical College of Wisconsin, Milwaukee, WI
Eric Gros
GE Healthcare, Waukesha, WI
Scott G. Baginski
Department of Radiology, Medical College of Wisconsin, Milwaukee, WI
Zachary R. Laste
Department of Radiology, Medical College of Wisconsin, Milwaukee, WI
Naveen M. Kulkarni
Department of Radiology, Medical College of Wisconsin, Milwaukee, WI

Darin Okerlund
GE Healthcare, Waukesha, WI
Taly G. Schmidt
Department of Biomedical Engineering, Marquette University and Medical College of Wisconsin, Milwaukee, WI

Abstract

Purpose

This study developed and validated a Motion Artifact Quantification algorithm to automatically quantify the severity of motion artifacts on coronary computed tomography angiography (CCTA) images. The algorithm was then used to develop a Motion IQ Decision method to automatically identify whether a CCTA dataset is of sufficient diagnostic image quality or requires further correction.

Method

The developed Motion Artifact Quantification algorithm includes steps to identify the right coronary artery (RCA) regions of interest (ROIs), segment vessel and shading artifacts, and to calculate the motion artifact score (MAS) metric. The segmentation algorithms were verified against ground-truth manual segmentations. The segmentation algorithms were also verified by comparing and analyzing the MAS calculated from ground-truth segmentations and the algorithm-generated segmentations. The Motion IQ Decision algorithm first identifies slices with unsatisfactory image quality using a MAS threshold. The algorithm then uses an artifact-length threshold to determine whether the degraded vessel segment is large enough to cause the dataset to be nondiagnostic. An observer study on 30 clinical CCTA datasets was performed to obtain the ground-truth decisions of whether the datasets were of sufficient image quality. A five-fold cross-validation was used to identify the thresholds and to evaluate the Motion IQ Decision algorithm.

Results

The automated segmentation algorithms in the Motion Artifact Quantification algorithm resulted in Dice coefficients of 0.84 for the segmented vessel regions and 0.75 for the segmented shading artifact regions. The MAS calculated using the automated algorithm was within 10% of the values obtained using ground-truth segmentations. The MAS threshold and artifact-length thresholds were determined by the ROC analysis to be 0.6 and 6.25 mm by all folds. The Motion IQ Decision algorithm demonstrated 100% sensitivity, 66.7% ± 27.9% specificity, and a total accuracy of 86.7% ± 12.5% for identifying datasets in which the RCA required correction. The Motion IQ Decision algorithm demonstrated 91.3% sensitivity, 71.4% specificity, and a total accuracy of 86.7% for identifying CCTA datasets that need correction for any of the three main vessels.

Conclusion

The Motion Artifact Quantification algorithm calculated accurate (<10% error) motion artifact scores using the automated segmentation methods. The developed algorithms demonstrated high sensitivity (91.3%) and specificity (71.4%) in identifying datasets of insufficient image quality. The developed algorithms for automatically quantifying motion artifact severity may be useful for comparing acquisition techniques, improving best-phase selection algorithms, and evaluating motion compensation techniques.

1 Introduction

Coronary computed tomography angiography (CCTA) is a noninvasive cardiac imaging exam for coronary artery disease diagnosis, in which iodinated contrast agent is intravenously injected to enhance the coronary arteries. From the CT scan, high resolution 3D image datasets can be reconstructed to visualize coronary arteries and to assess stenosis and disease level.[1]

Because CCTA images are collected while the heart is moving, motion artifacts may degrade the visualization of the vessels, which may make the dataset nondiagnostic. New CT scanners are designed to improve temporal resolution, as temporal resolution is a bottleneck of cardiac imaging. Despite technological advancements such as wide cone-beam coverage,[2], [3] fast gantry rotation times,[4] dual source scanners,[5] retrospective and prospective gating methods,[6] and best-phase selection algorithms,[7]-[9] reconstructing artifact-free coronary CT images is not always possible. For example, when heart rate exceeds 75 beats per min, the velocity at the lowest motion phase is significantly higher than that of patients with lower heart rate.[10] Motion correction algorithms have been proposed and clinically implemented to reduce residual motion artifacts. One correction approach uses motion artifacts metrics (MAM) to quantify image quality and then optimizes the CT reconstruction based on a MAM gradient descent procedure.[11] Another approach characterizes artery motion by a bidirectional label point matching method and then compensates the motion to a target phase during reconstruction.[12]

The purpose of this study was to develop and validate algorithms that automatically quantify the level of coronary artery motion artifact in clinical CCTA image sets. The algorithms developed in this work could be applied to identify the low-motion phase, optimize and evaluate motion compensation methods, or to quantitatively assess motion reduction techniques on clinical CCTA images. Motion artifact quantification is based on the product of two vessel motion artifact metrics validated in a previous study: fold overlap ratio (FOR) and low-intensity region score (LIRS).[13] The FOR metric quantifies the level of vessel deformation, while the LIRS metric quantifies the severity of the low-intensity shading artifacts. Previous studies proposed and validated metrics for relative motion artifact quantification across different phases of the same exam. Instead, the FOR and LIRS metrics were designed and validated for absolute quantification of motion artifact levels across different patient studies with varying characteristics such as vessel size, vessel contrast, image noise, and image resolution. The ability to quantify absolute motion artifact level enables several potential applications, for example evaluating motion reduction techniques across a range of patients and scanners.

In the previous study, the FOR and LIRS metrics were validated using gold standard, manually segmented vessel and artifact regions. In this current study, algorithms are developed and verified to automatically calculate the motion artifact metrics. These consist of algorithms to identify the slices that contain through-plane arteries, segment artery regions, and segment shading artifact regions. The developed algorithms are combined with the previously validated motion artifact metrics to create a Motion Artifact Quantification algorithm that outputs a motion artifact score (MAS) for each image slice.

While the proposed Motion Artifact Quantification algorithm has several potential applications, in this work the method is applied to the specific example of classifying CCTA datasets as either adequate diagnostic quality or requiring additional motion correction. This automated Motion Image Quality Decision algorithm could be beneficial for task-based assessment of motion correction techniques. The

automated motion artifact decision method could also improve workflow by enabling automatic application of motion correction only for datasets that need correction, while minimizing computation time for studies of adequate diagnostic quality. For example, previously proposed motion correction algorithms require multiple or iterative reconstructions that may be time consuming.[11], [12] The performance of the Motion IQ Decision method, based on the Motion Artifact Quantification algorithm, is evaluated in this work through an observer study.

The paper describes the Motion Artifact Quantification algorithm in Section 1 and the Motion IQ Decision method in Section 2. The image data used in this paper and verification/validation methods are described in Section 2.A.. Section 2.B. presents the results followed by discussion (Section 2.C.) and conclusions (Section 3).

2 Motion Artifact Quantification algorithm

A previous study demonstrated that the fastest coronary artery velocity was measured on right coronary artery (RCA) segments in which the vessel orientation was perpendicular to the slice plane (i.e., through-plane segment).[10] Therefore, this paper develops the Motion Artifact Quantification and Motion IQ Decision algorithms for image slices that contain the through-plane RCA, assuming that this vessel segment represents the motion artifacts level for the entire cardiac region. This assumption is tested by the observer study which is described in Section 2.C..

Figure 1 presents a flow chart of the proposed, automated Motion Artifact Quantification algorithm. The input to the algorithm is a CCTA image volume at one phase. The outputs are the motion artifact scores calculated for each image slice that contains the through-plane RCA.

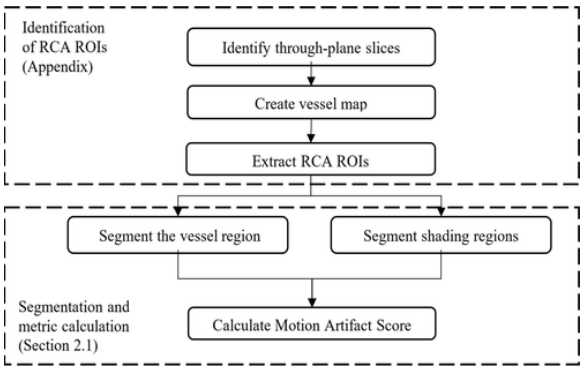

Figure 1 Motion Artifact Quantification algorithm flowchart.

To calculate the motion artifact metrics on through-plane RCA slices, an algorithm is first needed to identify the through-plane RCA location on each slice, after which regions of interest (ROIs) containing the RCA are extracted. RCA segmentation algorithms have been previously proposed and could be used for this purpose of the algorithm.[14]-[17] In this work, we developed an automated algorithm that leverages image processing steps developed in a previous study on identification of CCTA best phase.[9] The developed automated algorithm to identify ROIs containing the through-plane RCA is described in the **Appendix**. Figure 2 presents an example RCA ROI extracted by the algorithm.

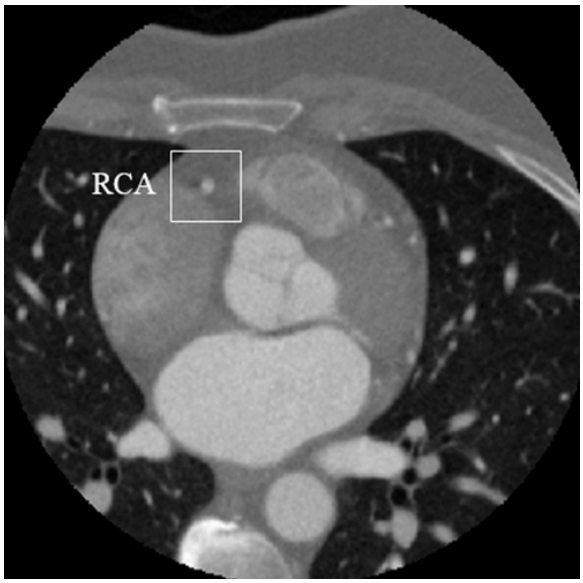

Figure 2 Example of extracted RCA ROI delineated by the white box.

Once the RCA ROIs have been extracted, the algorithm segments the vessel and shading artifact regions within the ROIs, as these regions are needed for calculating the motion artifact metrics. The vessel and shading region segmentation algorithms (Sections **2.A** and **2.B**) are novel steps of the Motion Artifact Quantification algorithm presented in this work to enable automated calculation of the motion artifact metrics. The last step of the Motion Artifact Quantification algorithm calculates the MAS for each ROI. The specific algorithm steps for this stage of the algorithm are described in more detail in the following sections.

2.A. Segment the vessel region

The input to this step of the algorithm is the ROI containing the through-plane RCA for each image slice, as shown in Fig. **1**. The output of this step is a binary mask corresponding to the vessel region, which includes regions of vessel deformation and vessel blur due to motion. Segmentation of the vessel region within the vessel ROI is required for calculating the FOR metric of vessel symmetry, which is part of the overall MAS.

Segmentation of the RCA vessel region in each ROI is performed using a K-means clustering algorithm. We assume that the RCA ROI images contain regions of the vessel, cardiac chambers, low-intensity shading artifacts, myocardium, and lung. Therefore, all pixel intensities in the RCA ROI are classified into one of four clusters: low-intensity pixels (lung and low-intensity shading artifacts), myocardium, high-intensity pixels (vessel; cardiac chamber; ribs and sternum), and intermediate-intensity pixels. The cluster mean values are initialized at −200 HU for the low-intensity cluster, 50 HU for the myocardium cluster, and the CT number of the identified RCA location for the high-intensity cluster. The mean of the intermediate-intensity cluster is initialized as the average of the initial means for the myocardium and high-intensity clusters. The intermediate-intensity cluster may contain part of the chambers in addition to the region of the RCA that is blurred due to motion. The purpose of the intermediate-intensity cluster is to break the connection between the RCA and the chambers in the high-intensity tissue cluster, as shown in Figs. **3**(b) and **3**(c). The K-means algorithm is performed for 10 iterations.

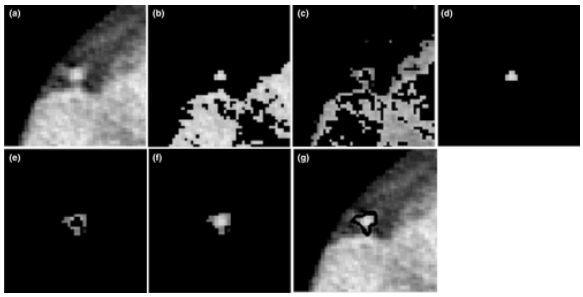

Figure 3 Example demonstrating the steps of vessel region segmentation algorithm. (a) Original image, (b) K-means clustering output corresponding to the high-intensity cluster, and (c) K-means clustering output corresponding to the intermediate-intensity cluster. (d) Depicts the vessel core region identified as the center region of (b). (e) Presents the intermediate-intensity region after an AND operation with the dilated vessel core region, representing the vessel motion blur. (f) is the final segmented vessel region, including the contributions of both the (d) vessel core and (e) motion blur. (h) Depicts the final segmented region as black contour overlaid on the RCA ROI.

Since the goal of this step of the algorithm is to generate a binary mask representing the vessel region, the low-intensity and myocardium clusters are ignored. Figures **3**(b) and **3**(c) depict the pixels within the clusters identified as "high intensity" and "intermediate intensity", which are further processed through morphological operations, as illustrated in Fig. **3**.

First, we perform connected components analysis on the regions identified in the high-intensity cluster. The component that contains the identified RCA location is selected as the vessel core region, as illustrated in Fig. **3**(d). To identify regions of the vessel that have been blurred due to motion, a vessel mask is first obtained by dilating the vessel core region with a disk shape kernel, with radius, *d*, that is equal to *c* times that of the RCA core equivalent radius:

$$d = c\sqrt{A_{vc}/\pi},$$
$$d = c\sqrt{A_{vc}/\pi}, \quad (1)$$

where A_{vc} is the number of pixels in the segmented vessel core and *c* is a scaling coefficient. To identify regions of the intermediate-intensity vessel that correspond to vessel blur, an AND operation is then performed between the vessel mask and the binary region representing the intermediate-intensity cluster, as depicted in Fig. 3(e). As *c* increases, more motion blur regions may be identified, but with the risk of erroneously including other tissues such as the myocardium or chambers. In this study, the scaling factor *c* was empirically set to 1.5. The final vessel region is equal to the union of the vessel core region [Fig. 3(d)] and the processed motion blur region [Fig. 3(e)], with results shown in Figs. 3(f) and 3(g). Figure 4 presents five examples of vessel region segmentation results.

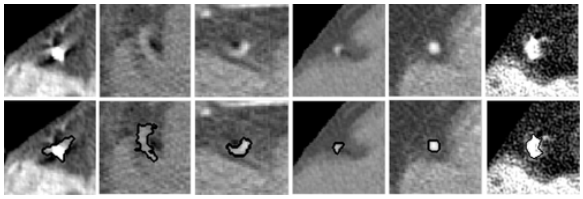

Figure 4 Examples of RCA segmentation results for five different vessel ROIs. The top row displays the original RCA ROI images. The bottom row marks the segmented RCA regions with contours. The first five columns demonstrate RCA

segmentation results with various motion artifact level. The last column demonstrates segmentation for a dataset with high noise level (84 HU noise standard deviation in the myocardium region).

2.B. Segment the low-intensity regions

Segmentation of the low-intensity shading regions within the vessel ROI is required for calculating the LIRS metric, which is part of the overall MAS. The output of this step is a binary mask corresponding to low-intensity shading artifacts. The K-means clustering algorithm described in Section **2.A** was not designed to distinguish the low-intensity shading artifacts from other low-intensity pixels in the ROI. Therefore, a combination of thresholding and morphological operations was developed to detect and segment the low-intensity shading regions.

As described in **Appendix I**, the first step of the RCA identification algorithm is to segment the cardiac region from the CT image slice, using a previously proposed algorithm.**9** The resulting cardiac region is used in the current step of the algorithm to exclude from analysis all pixels within the identified RCA ROI that are outside of the cardiac region. Within the RCA ROI, of the pixels within cardiac region, the pixels representing the myocardium are identified as having intensity less than 50 HU. The mean intensity of the identified myocardium pixels $\bar{I}_{myo}$ will be used to calculate LIRS metric in Section **2.C**. The pixels representing candidate low-intensity shading artifacts within the myocardium are identified as having intensity below the threshold T_{LIR}, which is calculated from the mean and standard deviation of the myocardium pixel intensities, $\bar{I}_{myo}$ and σ_{myo}, as

$$T_{LIR} = \bar{I}_{myo} - 1.5\sigma_{myo}$$
$$T_{LIR} = \bar{I}_{myo} - 1{:}5\sigma_{myo} \quad (2)$$

Candidate low-intensity shading pixels within a distance of 1.5 times the equivalent vessel radius are identified as shading artifacts, where the equivalent radius is calculated as

$$r = \sqrt{A_v/\pi}$$
$$r = A_v/\pi \quad (3)$$

where A_v is the area of the segmented RCA region in Section 2.A (i.e., sum of the pixels in the binary RCA mask). The result is the final mask of the low-intensity shading artifact regions, as demonstrated in Fig. 5.

Figure 5 Examples of LIR segmentation results. Top row displays the original RCA ROI images. The bottom row marks the segmented low-intensity shading regions with white contours. The first five columns demonstrate low-intensity shading segmentation results with various motion artifact level. The last column demonstrates segmentation for a dataset with high noise level (84 HU noise standard deviation in the myocardium region).

2.C. Calculate motion artifact score

A previous study proposed and validated two metrics, FOR and LIRS, to measure vessel deformation and shading artifacts, respectively.[13] We briefly summarize the metrics here, while additional details can be found in our previous study.

The FOR metric measures vessel symmetry within an ROI by "folding" the vessel region mask about two perpendicular axes. The ratio of the intersection and union of the two folded subsets is a measure of symmetry about each axis. For a perfectly symmetric region, the intersection and union of the folded subsets is equal. If the region is asymmetric about the folding axis, the intersection is less than the union, resulting in a ratio less than one. In the previous study, folding was performed across the vertical and horizontal axes, and the FOR metric was defined as the minimum of the two calculated ratios, with a range of 0 (no symmetry) to 1 (perfect symmetry). Since the FOR metric is only determined by vessel shape and is independent of vessel diameter, intensity, location, and other factors, it is designed to quantify absolute motion artifact level across different patients and scans.[13]

The LIRS metric measures low-intensity shading artifacts. The LIRS is defined as the average of two scores measuring shading intensity (LIR-*IS*) and area (LIR-*AS*), respectively. The intensity score is the ratio of the mean intensity of the shading region, T_{LIR}, to the mean intensity of the myocardium region, $\bar{I}_{myo}$, where both values have been offset by 1024 to ensure positive mean numbers, as described in Eq. [4]. The myocardium intensity, $\bar{I}_{myo}$, was identified and calculated as described in Section [2.B].

$$L_{LIR\_IS} = \frac{\bar{I}_{LIR} + 1024}{\bar{I}_{myo} + 1024}$$

$$L_{LIR\_IS} = \frac{\bar{I}_{LIR} + 1024}{\bar{I}_{myo} + 1024} \quad (4)$$

The Low-Intensity Region *Area Score* (LIR-*AS*) is defined as

$$L_{LIR\_AS} = 1 - \frac{A_{LIR}}{A_v}$$

$$L_{LIR\_AS} = 1 - \frac{A_{LIR}}{A_v} \quad (5)$$

where A_{LIR} is the total area of the low-intensity shading region mask, and A_v is the area of the segmented vessel region. Since the low-intensity shading region is usually smaller than the vessel region, LIR-*AS* ranges from 0 to 1, with 1 indicating a region without dark shading artifact. The final LIRS metric, which is the average of the LIR-*IS* and LIR-*AS* scores, has a range of (0, 1], with 0 corresponding to severe artifact and 1 corresponding to no artifact. Normalizing the shading intensity by the myocardium intensity and the shading area by the vessel area, enables the LIRS to quantify absolute motion artifact level across different patients.[13]

Although motion artifacts are characterized as vessel deformation and shading artifacts, the two types of artifacts may not always be present in an image. To more accurately quantify motion artifacts, the overall MAS was proposed in previous work as the product of the FOR and LIRS metrics.[13] This MAS metric was found to have good ranking agreement to observer scores in our previous study, and improved performance compared to the individual metrics.

3 Application of Motion Artifact Quantification algorithm to Motion IQ Decision method

The Motion Artifact Quantification algorithm outputs the MAS values for each through-plane slice. The Motion IQ Decision method performs additional processing to determine whether the entire dataset is of adequate image quality or requires further motion correction.

Motion artifacts may appear on every slice of a vessel or only a segment of the vessel. Either condition can cause the dataset to be nondiagnostic and require motion artifact correction. Therefore, the Motion IQ Decision algorithm is designed to identify vessel segments with unsatisfactory image quality and then to determine whether the length of the degraded vessel is large enough to cause the dataset to be nondiagnostic.

In the first step of the algorithm, the MAS score in each slice is compared with a threshold T_{MAS}. Slices with MAS less than T_{MAS} are identified as containing severe motion artifacts. If there are N continuous slices that are identified as containing severe artifacts, each with slice thickness of w mm, then this dataset contains a segment of length of $L = wN$ with severe motion artifacts. This study adopts the criteria that the dataset is of inadequate image quality (i.e., needs correction) if the length of RCA with severe motion artifacts (MAS < T_{MAS}) is more than a threshold, $L > T_{L\_RCA\_MAS}$. $T_{L\_RCA\_MAS}$ is referred to as artifact-length threshold in this study.

The T_{MAS} and $T_{L\_RCA\_MAS}$ threshold values were determined by receiver operating characteristic (ROC) techniques in this study using the results of an observer study as ground truth. The observer study and ROC analysis will be described in Sections **4.A** and **4.C**, respectively.

4 Evaluation methods

4.A. Clinical datasets and observer study

Twenty-three CCTA exams were used in this study to validate the Motion IQ Decision algorithm. The patient heart rates ranged from 52 to 82 bpm. The exams were collected with a 256-row CT scanner (GE Healthcare, Revolution CT, Chicago, USA) operating in axial scan mode. The images were acquired at 100 kVp or 120 kVp tube voltage, depending on patient size, with automatic tube current modulation and exposure control. Gantry speed was 0.35 s per rotation. The images were reconstructed by filtered backprojection, onto 17 to 26 cm fields of view with 512 × 512 pixels and a slice thickness of 0.625 mm. The SmartPhase technique (GE Healthcare) was applied to automatically identify the systolic and/or diastolic phases with lowest motion for each of the exams,[9] resulting in 30 total CCTA datasets. The identified lowest motion phases ranged from 43% to 82% of the R–R interval. The noise level of the 30 datasets was evaluated by calculating the standard deviation of a manually selected ROI within the myocardium on the center slice of each dataset. The minimum, average, and maximum standard deviation of the myocardium ROIs were 30.0, 46.3, and 84.4 HU. Three datasets contained minor or moderate stenosis, while six datasets contained no stenosis, as evaluated by a

board-certified radiologist specializing in cardiothoracic imaging. The stenosis level of 21 datasets could not be determined due to motion artifacts. The contrast of three exams was determined as fair or poor by the expert reader, while the remainder of the exams was considered to have adequate contrast. No datasets were excluded due to image quality or stenosis level. The Motion Artifact Quantification analysis was performed on reconstructed image slices with 0.625-mm slice thickness.

The 30 CCTA datasets, each consisting of a volume of images at one phase, were evaluated independently by three board-certified radiologist readers specializing in cardiothoracic or body imaging. For each dataset, the readers were asked to decide whether each dataset was of sufficient diagnostic motion artifact image quality or required additional motion correction for each coronary artery. The majority opinion of the readers for each coronary artery was considered as the ground-truth decision.

4.B. Verification of segmentation methods

Three CCTA exams were used to verify the vessel and shading segmentation algorithms presented in Section **2.A** and **2.B**, respectively. Twenty RCA ROIs were randomly selected for this verification study, as shown in Fig. **6**. The 20 ROIs contain varying degrees of motion artifacts.

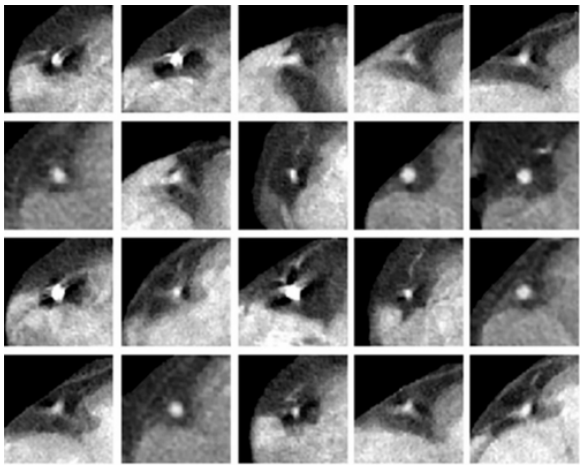

Figure 6 RCA ROIs used for segmentation verification.

Three readers, trained in biomedical engineering, manually segmented both the deformed vessel and the low-intensity shading regions for each RCA ROI. The three reader segmentations were combined into a ground-truth segmentation using the Simultaneous Truth and Performance Level Estimation (STAPLE) method, with a probability threshold of 0.9.**18**

For each ROI, the vessel and shading regions were segmented by the algorithms described in Section **1**, then compared with ground-truth segmentations using the Dice coefficient metric.

In addition to quantifying the segmentation performance, an investigation was performed to evaluate the effect of the automated segmentation algorithm on the calculation of the MAS metric. The MAS metric was calculated using both the ground-truth segmented regions and the algorithm-segmented regions, denoted as MAS_{Gi} and MAS_{Ai} respectively, where i = 1, 2, …, 20 is the image index. To quantify the effect of the automated segmentation algorithms on the calculation of the metrics, the difference

between the metrics calculated using the ground-truth and algorithm-generated segmentations was calculated as:

$$D_i = MAS_{Gi} - MAS_{Ai}$$
$$D_i = MAS_{Gi} - MAS_{Ai} \quad (6)$$

which is referred to as the MAS difference. If the algorithm-generated segmentations are identical to the ground-truth segmentations, the MAS difference is zero. The MAS difference distribution of the 20 RCA ROIs was fit to a normal distribution. The mean of the fitted normal distribution indicates whether the segmentation algorithm introduces a bias in the MAS calculation. The standard deviation of the fitted normal distribution quantifies the variation in MAS due to segmentation errors. This study used the 95% confidence interval of the fitted normal distribution as a measure of precision.

4.C. Cross-validation ROC analysis to identify Motion IQ Decision algorithm thresholds

In this study, a five-fold cross-validation method was used to both identify the thresholds of the Motion IQ Decision algorithm (training) and to evaluate the algorithm performance (testing). Compared with simply dividing the datasets into a training set and test set, the cross-validation method utilizes all of the datasets for both training and evaluation, thereby more reliably estimating classifier performance from a limited number of datasets.[19]

The five-fold cross-validation method used in this study randomly split the 30 datasets into five distinct sets with stratified sampling, which means that the ratio of the number of datasets that need correction to the number of datasets with adequate image quality for each fold was the same as the ratio for the total dataset. The following ROC analysis was performed for five trials, with four folds (24 datasets) selected for training each time. For each trial, the 24 training datasets were used to determine the Motion IQ Decision algorithm thresholds, T_{MAS} and $T_{L\_RCA\_MAS}$ by ROC techniques. For each trial, the remaining fold (six datasets) was used to verify the Motion IQ Decision algorithm performance using the method described in Section **4.D**.

The training datasets were input to the Motion Artifact Quantification algorithm, which output the MAS score for each image slice in the training dataset identified by the algorithm as containing the through-plane RCA. The Motion IQ Decision algorithm was performed with the MAS threshold, T_{MAS}, varied between 0 to 1 with an increment of 0.05, and the threshold corresponding to the length of motion artifact segment, $T_{L\_RCA\_MAS}$, fixed at 3.75 mm. Datasets were identified by the algorithm as being of inadequate image quality ("needing correction") if the MAS was less than T_{MAS} for a vessel segment of length greater than $T_{L\_RCA\_MAS}$. The algorithm decision of whether the dataset was of adequate image quality was compared to the majority reader opinion for the RCA vessel, with true positives, true negatives, false negatives, and false positive results defined in Table 1. The true positive rate (TPR) was calculated as the ratio of true positive to all positive results determined by the readers, and the false positive rate (FPR) was calculated as false positive results divided by all negative results determined by the readers.

Table 1. True condition and predicted condition definition for Motion IQ Decision algorithm validation

	Algorithm results	
	RCA needs correction	**Adequate RCA IQ**

Readers' decisions		
RCA needs correction	True Positive (TP)	False Positive (FP)
Adequate RCA IQ	False Negative (FN)	True Negative (TN)

Both true positive and true negative results are correct decisions, thus the accuracy was defined as the sum of true positive and true negative results divided by the total number of studies. The ROC curve was generated by plotting the TPR vs the FPR for each T_{MAS} threshold value.

The ROC analysis was then repeated with the $T_{L\_RCA\_MAS}$ fixed at each of 5, 6.25, and 7.5 mm, with the T_{MAS}, varied between 0 to 1. The tested $T_{L\_RCA\_MAS}$ range of 3.75 to 7.5 mm was selected as it represents the segment length of small lesions.[20] For each ROC curve, the point which gave the highest accuracy, that is, the highest sum of true positive and true negative results, was selected as the optimal T_{MAS} setting for that specific motion artifact-length threshold setting.

For each of the five-fold trails, the ROC curve with the highest accuracy was identified, and the corresponding highest accuracy combination of $T_{L\_RCA\_MAS}$ and T_{MAS} thresholds was identified as the final Motion IQ Decision thresholds for each of the five-fold trials.

4.D. Evaluation of the Motion IQ Decision algorithm

The Motion IQ Decision algorithm was developed assuming that the RCA represents the motion artifact severity for the entire CCTA exam. The Motion IQ Decision algorithm was first verified for its performance in identifying datasets with insufficient RCA image quality, using the five-fold cross-validation method. For each of the fivefold trials, the algorithm decision for the six testing datasets was compared to the ground-truth expert decisions for the RCA. Sensitivity, specificity and overall accuracy were calculated as metrics of Motion IQ Decision Algorithm performance for each fold. The mean and standard deviation of the sensitivity, specificity, and accuracy were calculated to characterize the overall algorithm performance. The final $T_{L\_RCA\_MAS}$ and T_{MAS} thresholds were selected as the mean of the thresholds determined by the five-fold trials.

The algorithm was then validated for its performance identifying datasets with insufficient CCTA image quality using all 30 datasets for testing. For this validation study, the ground-truth decision of "needs correction" was determined if at least one of the vessels was identified as requiring correction by a majority of the readers. The ground-truth decision that considered all three vessels was compared to the decision output by the Motion IQ Decision algorithm for the RCA. In this study, the readers' decisions for all three vessels were used to validate the assumption that the RCA represents the motion artifact level of the whole CCTA dataset.

5 Results

5.A. Verification of the vessel and shading artifact region segmentation algorithms

Figure [7] displays the ground-truth and algorithm segmentations of the ROI RCAs used for segmentation verification, with the Dice coefficients also displayed for each ROI. The mean Dice coefficient of agreement between the algorithm-generated and ground-truth vessel regions was 0.84 across the 20 ROIs. Four of the investigated ROIs did not have low-intensity shading artifacts identified by the readers or algorithm. The mean Dice coefficient of the low-intensity shading artifact region across the remaining 16 ROIs was 0.75.

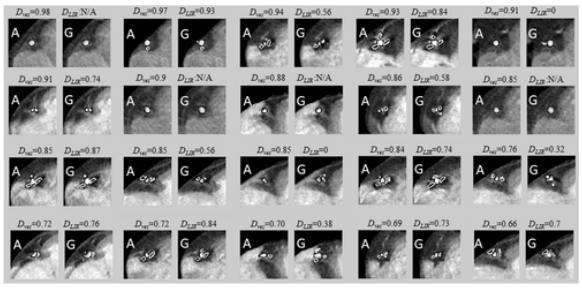

Figure 7 Verification results of the algorithms to segment the vessel and low-intensity shading regions. For each pair of images, the left image shows the segmented region output by the algorithm, labeled with "*A*", and the right image shows the ground-truth segmentation, labeled with "*G*". Segmented vessels are marked with black contours, and low-intensity shading regions are marked with white contours. Dice coefficients of vessel segmentation (D_{ves}) and low-intensity shading region segmentation (D_{LIR}) are displayed at the top of the image pairs.

The distribution of differences between the MAS calculated using the algorithm and ground-truth segmentations was fit to a normal distribution and found to have a mean of 0.06 and standard deviation of 0.1, as plotted in Fig. 8. The 95% confidence interval was found to be between 0.016 and 0.104, suggesting that the segmentation algorithm resulted in less than 10% MAS estimation error, relative to the full MAS range.

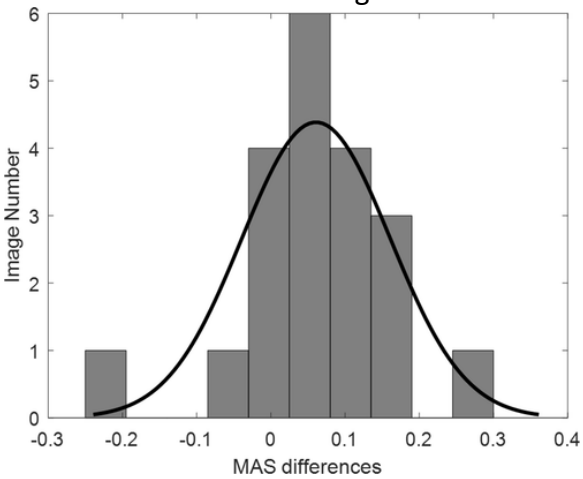

Figure 8 The histogram of the difference in MAS values calculated using the ground-truth and algorithm-generated segmentations for 20 RCA ROIs. The fitted normal curve is also displayed.

That the mean MAS difference across the 20 ROIs was greater than zero (0.06) demonstrates that the MAS calculated using ground-truth segmentation is, on average, 6% higher than that calculated using the automated-algorithm segmentation. Since a lower MAS represents more severe artifacts, this positive mean difference signifies that the automated segmentation overestimates the level of artifact severity by 6% on average. Further analysis calculated the difference in the FOR metrics obtained using ground-truth and algorithm segmentations and the differences in the LIRS metric obtained using ground-truth and algorithm segmentations. The mean FOR difference of the 20 ROIs was −0.01, while mean LIRS difference was 0.07. Therefore, the MAS offset was mainly caused by the automated segmentation algorithm detecting more shading artifacts than the ground-truth segmentations.

5.B. Examples of motion artifact quantification

The Motion Artifact Quantification algorithm outputs the MAS for every slice that contains the through-plane RCA, with an MAS = 1 indicating no motion artifacts and MAS = 0 indicating severe motion artifacts. Figures 9 and 10 are examples of Motion Artifact Quantification algorithm results for varying levels of motion artifact. Figure 9 presents an example of a dataset with generally low-motion artifacts, for which the MAS across all slices ranged from 0.21 to 0.88. Mean and standard deviation of the MAS across all slices were 0.66 and 0.14, respectively. The distal segment of the RCA in Fig. 10 contains more severe motion artifacts than the proximal segment. The mean MAS of the proximal 15 slices was 0.44, which was higher than the mean MAS of 0.31 for the distal 19 slices. Overall, the examples Figs. 9 and 10 demonstrate a range of motion artifact levels across different patients, from low (Fig. 9) to medium (proximal segment of Fig. 10) to high motion artifacts (distal segment of Fig. 10). Accordingly, the mean MAS of these datasets/segment were, respectively, 0.66, 0.44, and 0.31, which generally matched the perceived level of motion artifact.

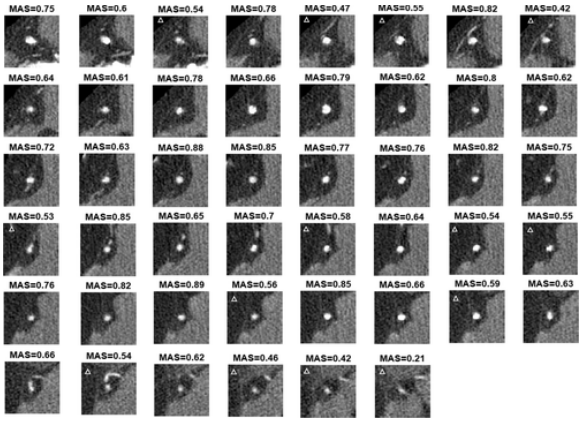

Figure 9 The first example of Motion Artifact Quantification and Motion IQ Decision results on one dataset. This figure shows the RCA ROIs on every other through-plane slice with the left-top ROI displaying the most superior slice. The MAS is labeled on top of each ROI. The RCA ROIs marked with a triangle were determined as "contain severe motion artifacts" by Motion IQ Decision algorithm as the MAS were less than the TMAS threshold of 0.6. This dataset contains low level of motion artifacts and was determined as having sufficient image quality for diagnosis by both the readers and Motion IQ Decision algorithm.

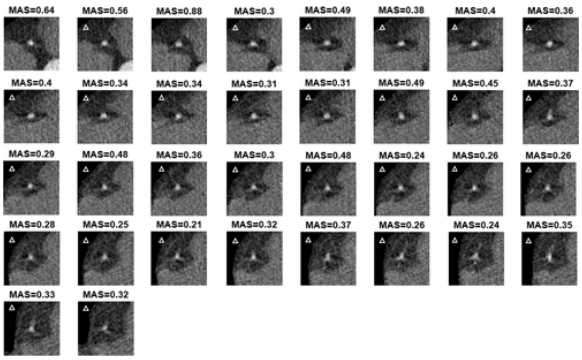

Figure 10 The second example of Motion Artifact Quantification and Motion IQ Decision results on one dataset. This figure shows the RCA ROIs on every other through-plane slice with the left-top ROI displaying the most superior slice. The MAS is labeled on top of each ROI. The MAS is labeled on top of each ROI. The RCA ROIs marked with a triangle were determined as "contain severe motion artifacts" by Motion IQ Decision algorithm as the MAS was less than the T_{MAS} threshold of 0.6. The distal RCA segment contains high motion artifacts, while the proximal segment image quality is relatively good. This dataset was determined as needing motion correction by both the readers and the Motion IQ Decision algorithm.

5.C. Cross-validation and Motion IQ Decision algorithm performance

The ROC curves of one fold trial resulting from the threshold parameters sweeps are shown in Fig. 11, with the artifact-length threshold ($T_{L\_RCA\_MAS}$) set to 3.75, 5, 6.25, and 7.5 mm in Figs. 11(a)–11(d). For each ROC curve, TPR and FPR were calculated with MAS threshold varied between to 0 to 1 with 0.05 step, that is, 21 points are on each ROC curve. In some cases, two thresholds resulted in the same TPR and FPR, causing the points to overlap on the curve. The solid point on each ROC curve is the one that gives the highest number of true positive plus true negatives, that is, the highest accuracy of the Motion IQ Decision. For this fold trail, T_{MAS} and $T_{L\_RCA\_MAS}$ combinations of (0.60, 6.25 mm) produced the highest accuracy of 87.5% for the 24 training datasets in this fold trial.

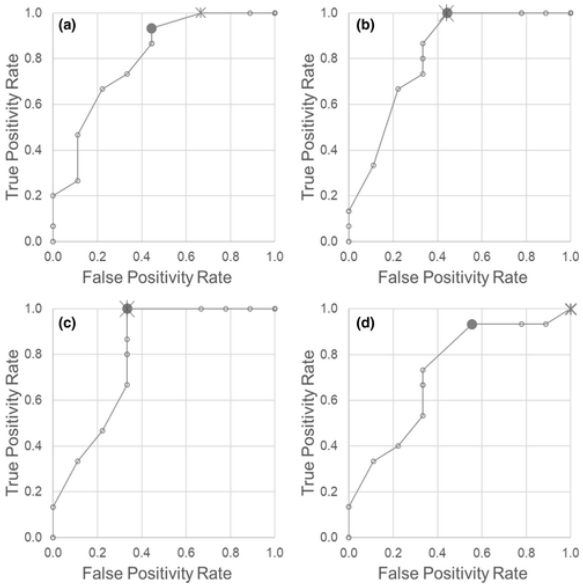

Figure 11 The ROC curves corresponding to artifact-length threshold values of (a) 3.75 mm, (b) 5 mm, (c) 6.25 mm, and (d) 7.5 mm for one fold. On each ROC curve, the solid marker represents the operating point with highest accuracy (the highest sum of true positive and true negative results). The asterisk marker corresponds to the lowest threshold that provides a sensitivity of one. The point with highest accuracy on plot (a) is (T_{MAS}, $T_{L\_RCA\_MAS}$) equal to (0.455, 3.75 mm), with accuracy of 79.2%. The highest accuracy points on (b) and (c) are both (0.60, 5 mm) with accuracy of 83.3% and 87.5%, respectively. The point with highest accuracy on plot (d) is *(T_{MAS}, $T_{L\_RCA\_MAS}$)* equal to (0.65, 7.25 mm), with accuracy of 75%.

The Motion IQ Decision algorithm may be useful as a task-based evaluation and comparison of different motion artifact reduction techniques. For this application, the thresholds that yield the highest accuracy are desired. Another potential application of the Motion IQ Decision algorithm is to automatically send datasets with insufficient image quality for motion correction, while saving the computation time if correction is not needed. When we select T_{MAS} and $T_{L\_RCA\_MAS}$ by the above "highest accuracy" strategy, some datasets that need correction are missed. Since the cost of missing a dataset that needs correction is greater than the cost of unnecessarily correcting a dataset, another option for this application is to adopt a "low-risk" strategy. This strategy selects the lowest T_{MAS} that yields a sensitivity of one. This low-risk strategy ensures that all datasets that require correction are identified although with a potential increase in the number of false negative datasets that will be unnecessarily corrected. The "low-risk" points on Fig. 11 are marked with asterisks. For Figs. 11(b) and 11(c), the highest accuracy strategy and the low-risk strategy selected the same operating point. The selected T_{MAS} and $T_{L\_RCA\_MAS}$ combination of (0.6, 6.25 mm) met both the highest accuracy strategy

and low-risk strategy, resulting in a sensitivity of 1.0. ROC curves similar to Fig. 11 were obtained during training of the other four fold trials. All five fold trials determined the same optimal combination of T_{MAS} and $T_{L\_RCA\_MAS}$ threshold values (0.6, 6.25 mm) as meeting both the highest accuracy and low-risk strategy.

Table 2 displays the sensitivity, specificity, and accuracy of the Motion IQ Decision algorithm in identifying datasets for which the RCA needs correction, using the six testing datasets for each of the five fold trials. All fold trials resulted in a sensitivity of 100%, demonstrating that the Motion IQ Decision can robustly identify the datasets of needing correction. The specificity was 66.7% ± 27.9%, with an accuracy of 86.7% ± 12.5%.

Table 2. Selected thresholds and test performance of five-fold cross-validation

	T_{MAS}	$T_{L\_RCA\_MAS}$ (mm)	Sensitivity (%)	Specificity (%)	Accuracy (%)
Fold #1	0.6	6.25	100	50	83.3
Fold #2	0.6	6.25	100	50	83.3
Fold #3	0.6	6.25	100	100	100
Fold #4	0.6	6.25	100	100	100
Fold #5	0.6	6.25	100	33.3	66.7
Mean	0.6	6.25	100	66.7	86.7
SD			0	27.9	12.5

Figures 9 and 10 demonstrate examples of Motion IQ Decision results. The first example was determined as “adequate RCA image quality” by the both the readers and the algorithm, while the second example was determined as “RCA needs correction” by readers and the algorithm.
Figure 12 presents one false negative result, for which the reader decision was “adequate RCA image quality” and the algorithm decision was “RCA needs correction,” because the length of the RCA that contained severe artifacts exceeded the artifact-length threshold of 6.25 mm. For this dataset, two readers determined that the RCA was of sufficient image quality, while the third reader determined it as needing correction. Because the low-risk strategy was adopted to determine the Motion IQ Decision parameters, the datasets without consensus among the readers are more likely determined as needing correction, as occurred for this one dataset.

Figure 12 Dataset for which Motion IQ Decision returned a false positive. This figure shows the RCA ROIs on every through-plane slice with the left-top ROI displaying the most superior slice. The MAS is labeled on top of each ROI. The RCA ROIs marked with a triangle were determined as “contain severe motion artifacts” by the Motion IQ Decision algorithm as the MAS values were less than the T_{MAS} threshold of 0.6. The readers identified

this dataset as sufficient image quality while Motion IQ Decision algorithm identified this dataset as needing correction as its length of "contain severe motion artifacts" was 16.875 mm, which was longer than the threshold of 6.25 mm.

The algorithms developed in this work assumed that the through-plane RCA segment represents the motion artifact level for all coronary arteries. The results of our current study suggest that this assumption is true most, but not all, of the time. Of the 23 datasets that were determined as needing correction by the readers, 20 were rated as needing correction for the RCA, while three datasets were rated as needing correction for only the left vessels, that is, 10% of datasets needed correction only for the left vessels. A CCTA dataset will need motion correction if any of the three coronary arteries needs correction. In the validation study, we compared the Motion IQ Decision algorithm decision, based on the RCA, with the ground-truth decision based on all three coronary arteries for all 30 datasets, as shown in Table 3. The Motion IQ Decision algorithm identified CCTA datasets that need correction with 91.3% sensitivity, 71.4% specificity, and a total accuracy of 86.7%.

Table 3. Motion IQ Decision algorithm validation results based on three coronary arteries

Readers' decision (number of datasets)		**Motion IQ decision output (number of datasets)**	
		Needs correction	**Adequate IQ**
Needs correction	23	21 (91.3%)	2 (8.7%)
Adequate IQ	7	2 (28.6%)	5 (71.4%)

6 Discussion

The purpose of this study was to (a) develop and evaluate algorithms to automatically quantify motion artifact metrics in clinical CCTA images and (b) apply the algorithms to identify CCTA datasets that need further correction. The results demonstrated that the automated segmentation algorithms developed in this work introduced less than 10% error in the final MAS compared to manual artifact segmentation. This error was primarily due to oversegmentation of the low-intensity shading regions, which demonstrated a lower Dice coefficient (0.75) than the vessel region segmentation algorithm (0.84). Therefore, the Motion Artifact Quantification algorithm could be improved in the future by increasing the accuracy of the low-intensity artifact segmentation step.

The assumption that the RCA represents the overall CCTA image quality was based on a previous study that demonstrated a higher velocity for the RCA than the left coronary artery velocities.[10] Of the 23 datasets in our study that were identified as needing correction, three of the datasets had severe artifacts in the left vessels but not the RCA. This is likely because factors other than velocity, including both patient and scanner factors, affect the motion artifact severity, for example vessel diameter, intensity, and gantry start angle. Also, if the left vessels contain calcifications, the high intensity may increase the perceived severity of motion artifacts. The severity of motion artifact also depends on the direction of the motion relative to the projection direction. The motion direction of the left anterior descending (LAD) and left circumflex (LCX) vessels may be such that the artifacts appear more severe for the left vessels than for the RCA, despite the potentially lower velocity of the left vessels. Quantifying the RCA motion may be sufficient for evaluating the performance of different motion artifact reduction techniques. For identifying CCTA datasets that require further correction, the results of our study suggest that the Motion IQ Decision algorithm could be improved by extending the algorithms to the left vessels.

One limitation of this work is that the all images were obtained by filtered backprojection reconstruction. Iterative reconstruction approaches may alter the noise and texture properties of the reconstructed images, which may affect the segmentation algorithms presented in Section 1. Future study is required to investigate the performance of the Motion Artifact Quantification algorithm for images reconstructed by iterative approaches.

Another limitation of this study is that none of the clinical datasets contained vessels with total occlusion. Therefore, performance of the Motion Artifact Quantification algorithm on slices with total occlusion is unknown. An occluded RCA may not be enhanced by contrast agent during the scan, which could cause the RCA identification and vessel map algorithms to identify an incorrect RCA ROI. An incorrect RCA ROI would result in erroneous FOR and LIRS values that do not represent the level of motion. The Motion Artifact Quantification algorithm could be improved by implementing criteria to exclude such slices from further analysis. Another potential issue is that the FOR metric cannot distinguish between vessels deformed by stenosis from vessels deformed by motion. It is possible that the FOR score for a stenosed vessel may be erroneously high, therefore overestimating the level of motion artifact for slices with stenosis. In this study, three datasets contained minor or moderate stenosis, while the stenosis level of 21 datasets could not be evaluated due to motion artifacts.

The robustness of the Motion Artifact Quantification algorithm and the Motion IQ Decision algorithm depends on multiple factors, including noise level, vessel size, contrast, and resolution. This study developed and verified the algorithms using datasets for which these factors were varied. For example, the image noise varied from 30.0 to 84.4 HU (myocardium ROI standard deviation). The pixels sizes of the datasets varied from 0.293 to 0.7031 mm, with a mean pixel size of 0.4156 mm. The contrast enhancement was rated as poor for three datasets. This study did not exclude any exams due to any image quality factors. The Motion IQ Decision algorithm correctly determined the need for motion correction for the three exams with poor or fair contrast and for the three exams with stenosis. The algorithm also made the correct decision for the exam with the highest noise level.

As described in Section 5.C, all five folds of the cross-validation study identified the same thresholds, T_{MAS} = 0.6 and $T_{L\_RCA\_MAS}$ = 6.25 mm, as meeting both the highest accuracy strategy and the lowest risk strategy. While these consistent values across validation folds suggest that these thresholds are fairly robust, training with more datasets may yield different threshold values. Additional testing datasets are needed for a larger scale study of algorithm performance across a larger range of clinical conditions and image quality factors.

This paper presents one potential application of the Motion Artifact Quantification algorithm—automatically determining whether a CCTA dataset is of sufficient image quality or requires additional motion correction. This Motion Check Decision algorithm could be used to streamline CCTA workflow. In addition, the presented algorithms could be used to improve best-phase selection algorithms and to evaluate motion reduction techniques. For example, for a specific motion compensation technique, the Motion IQ Decision algorithm could determine how often a particular motion correction technique improves the image quality from inadequate to adequate, thus providing a task-based evaluation.

7 Conclusion

This study developed and validated a series of algorithms to automatically quantify the level of motion artifact on clinical CCTA images. The study demonstrated that the automated segmentation algorithms developed in this work introduced less than 10% error in the final MAS compared to manual artifact segmentation. The Motion IQ Decision algorithm demonstrated 100% sensitivity, 83.3% specificity, and a total accuracy of 93.3% for identifying datasets in which the RCA required correction. The Motion IQ Decision algorithm, demonstrated 91.3% sensitivity, 71.4% specificity, and a total accuracy of 86.7% for identifying whole CCTA datasets that need correction. The developed algorithms for automatically quantifying motion artifact severity may be useful for comparing acquisition techniques, improving best-phase selection algorithms, and evaluation motion compensation techniques.

Acknowledgment

This study was funded in part by a research grant from GE Healthcare.

Conflicts of interest

Hongfeng Ma received research funding from GE Healthcare during the course of this project. Eric Gros and Darin Okerlund are employees of GE Healthcare. Taly Gilat Schmidt receives research funding from GE Healthcare.

Appendix I

Identification of RCA ROIs

As presented in Fig. 1, the RCA ROI identification algorithm consists of three steps: identify through-plane slices, create vessel map, and extract RCA ROIs. RCA segmentation algorithms have been previously proposed and could be used for this purpose of the algorithm.[14]-[16] In this work, we developed an automated algorithm that leverages image processing steps developed in a previous study on identification of CCTA best phase.[9] The RCA ROI identification algorithm begins with the vessel-enhanced images that were obtained by a sequence of cardiac-region segmentation, top hat transformation, Sobel filtering, and matched filtering, as described in the previous study.[9]

A1 Identify through-plane slices

The validated motion artifact metrics used in this study assume that the vessel is circular, which is true for slices in which the vessel orientation is primarily perpendicular to the slice plane (i.e., through-plane slices). Therefore, the first step is to identify the slices with through-plane vessels. To identify the through-plane slices, the algorithm first identifies the proximal and distal in-plane vessel sections, and assumes that the slices between the two sections are through-plane.

This algorithm takes advantage of the fact that that the extent of in-plane vessels within an image slice is greater than that of through-plane vessels. The algorithm begins with the vessel-enhanced images output by an algorithm developed in previous work.[9] Next, thin slab (5 mm) maximum intensity projections (MIP), centered on each image slice location, are created to further accentuate vessels with large in-plane extent. The intensities within the right half of each MIP image are summed to represent the in-plane extent of the vessels in that slice. An example of the MIP-sum per slice is plotted in Fig. 13. The algorithm identifies the two maximum peaks in the MIP-sum values, which represent the two in-plane vessel sections, and identifies the slices between the two peaks as containing the through-plane

RCA. Figure 14 demonstrates an example of the performance of the algorithm for the identification of through-plane slices on one volume dataset.

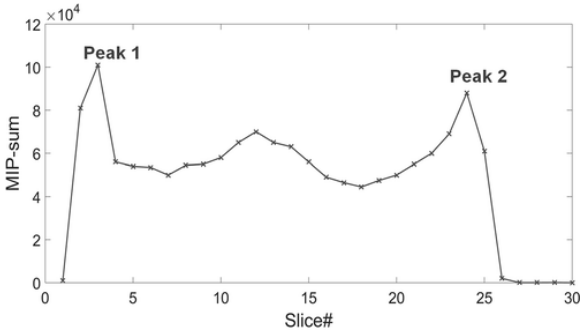

Figure 13 The MIP-sum is plotted against slice number for an example patient dataset. The two peak locations identified by the algorithm represent the two in-plane vessel section locations.

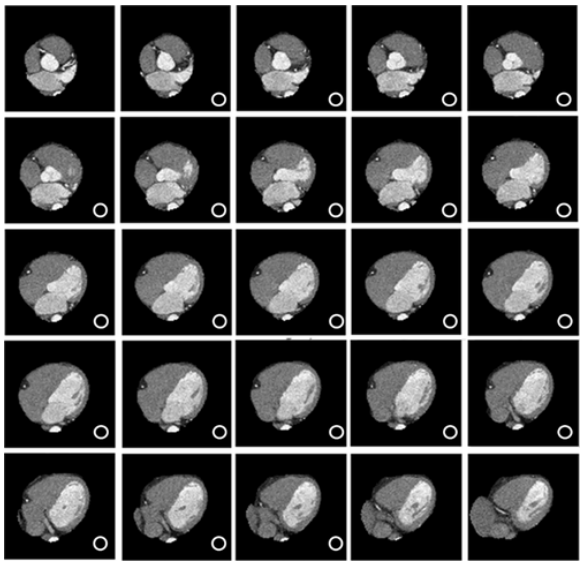

Figure 14 Example of identifying through-plane slices in one volume dataset. Only the segmented cardiac regions are displayed. The top left image is the most superior slice and the bottom right image is the most inferior slice. Slice thickness is 2.5 mm. The slices labeled with a circle were identified by the algorithm as containing through-plane vessels and were further processed in subsequent steps of the Motion Artifact Quantification algorithm.

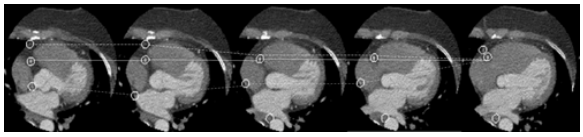

Figure 15 Demonstration of the vessel map algorithm. The three paths are built recursively from the three candidate points on the first slice. The RCA locations are identified by the solid path whose path length is the smallest. In this example, the RCA location is correctly identified by the algorithm in all slices.

A2 Create vessel map

The next step in the algorithm estimates the location of the RCA in each through-plane slice, resulting in the list of the RCA center pixel coordinates, which is referred to as the Vessel Map.

In our previous work, three candidate RCA locations in the right half of each image slice were identified by thresholding the vessel-enhanced images.9 Further analysis demonstrated that this method almost

always identified the correct RCA location as one of the three candidate locations, even in the presence of motion artifacts. Therefore, the goal of the vessel map algorithm developed in the current work is to select the correct RCA location from the three candidate points.
The proposed vessel map algorithm exploits the fact that the RCA vessel is continuous and that the Euclidean distance between the x–y plane coordinates of the RCA on adjacent slices should be small. The vessel map algorithm is performed with the following steps, as illustrated in Figure 15:

- Step 1: Starting with the first candidate location on the first slice, calculate the 2D Euclidean distance to each of the three candidate points on the next slice. The point located at the closest distance is considered to be connected to the candidate point on the first slice. From the selected point on the second slice, repeat the method to select the point on the third slice. This process is repeated for all slices. All identified points are considered to form a path, and the sum of the distances between points equals the path length.
- Step 2: Repeat Step 1 for the remaining two candidate points on the first slice. At the end of this step, there are three possible vessel paths, each with a calculated path length.
- Step 3: The RCA vessel map is identified as the path with shortest path length. The vessel map algorithm outputs the RCA locations (pixel coordinates) on each slice.

A3 Extract RCA ROIs

Regions of interest (ROI's) of size 15 × 15 mm^2 are extracted for each slice, centered on the RCA location identified on the vessel map. This ROI size was selected based on the expected maximum coronary artery diameter of 5 mm21 and so that in presence of motion artifacts, both the deformed RCA and shading artifacts are included in the ROI. Figure 2 presents an example of an output RCA ROI.

References

1Sun Z, Choo GH, Ng KH. Coronary CT angiography: current status and continuing challenges. Br J Radiol. 2012; 85: 495– 510.

2Elmquist R. The Impact of 320 Detector Rows: Aquilion ONE in the Pediatric Setting. Imaging Biz Electronic Journal for Leaders in Medical Imaging Services; 2009.

3Latif MA, Sanchez FW, Sayegh K, et al. Volumetric single-beat coronary computed tomography angiography: relationship of image quality, heart rate, and body mass index. Initial patient experience with a new computed tomography scanner. J Comput Assist Tomogr. 2016; 40: 763– 772.

4Russo V, Garattoni M, Buia F, Attinà D, Lovato L, Zompatori M. 128-slice CT angiography of the aorta without ECG-gating: efficacy of faster gantry rotation time and iterative reconstruction in terms of image quality and radiation dose. Eur Radiol. 2016; 26: 359– 369.

5Johnson TR, Nikolaou K, Wintersperger BJ, et al. Dual-source CT cardiac imaging: initial experience. Eur Radiol. 2006; 16: 1409– 1415.

6Desjardins B, Kazerooni EA. ECG-gated cardiac CT. Am J Roentgenol. 2004; 182: 993– 1010.

7Wick CA, McClellan JH, Arepalli CD, et al. Characterization of cardiac quiescence from retrospective cardiac computed tomography using a correlation-based phase-to-phase deviation measure. Med Phys. 2015; 42: 983– 993.

8Manzke R, Köhler T, Nielsen T, Hawkes D, Grass M. Automatic phase determination for retrospectively gated cardiac CT. Med Phys. 2004; 31: 3345– 3362.

9Stassi D, Dutta S, Ma H, et al. Automated selection of the optimal cardiac phase for single-beat coronary CT angiography reconstruction. Med Phys. 2016; 43: 324– 335.

10Husmann L, Leschka S, Desbiolles L, et al. Coronary artery motion and cardiac phases: dependency on heart rate—implications for CT image reconstruction. Radiology. 2007; 245: 567– 576.

11Rohkohl C, Bruder H, Stierstorfer K, Flohr T. Improving best-phase image quality in cardiac CT by motion correction with MAM optimization. Med Phys. 2013; 40: 031901.
12Iatrou M, Pack JD, Bhagalia R, Beque D, Seamans J. Coronary artery motion estimation and compensation: a feasibility study. In: IEEE Nuclear Science Symposium & Medical Imaging Conference; 2010.
13Ma H, Gros E, Szabo A, et al. Evaluation of motion artifact metrics for coronary CT angiography. Med Phys. 2018; 45: 687– 702.
14Zheng Y, Loziczonek M, Georgescu B, Zhou SK, Vega-Higuera F, Comaniciu D. Machine learning based vesselness measurement for coronary artery segmentation in cardiac CT volumes. In: Med Imaging: Image Processing; 2011.
15Yang Y, Tannenbaum A, Giddens D. Knowledge-based 3D segmentation and reconstruction of coronary arteries using CT images. Engineering in Medicine and Biology Society, 2004. IEMBS'04. 26th Annual International Conference of the IEEE. Vol. 1. IEEE; 2004.
16Wang C, Smedby O. An automatic seeding method for coronary artery segmentation and skeletonization in CTA. Insight J. 2008; 43: 1– 8.
17Babalola KO, Patenaude B, Aljabar P, et al. Comparison and evaluation of segmentation techniques for subcortical structures in brain MRI. In: International Conference on Medical Image Computing and Computer-Assisted Intervention. Heidelberg, Germany: Springer; 2008: 409– 416.
18Warfield SK, Zou KH, Wells WM. Simultaneous truth and performance level estimation (STAPLE): an algorithm for the validation of image segmentation. IEEE Trans Med Imaging. 2004; 23: 903– 921.
19Kohavi R. A study of cross-validation and bootstrap for accuracy estimation and model selection. In: Proceedings of the 14th International Joint Conference on Artificial Intelligence; 1995: 1137– 1143.
20Morice M-C, Colombo A, Meier B, et al. Sirolimus-vs paclitaxel-eluting stents in de novo coronary artery lesions: the REALITY trial: a randomized controlled trial. JAMA. 2006; 295: 895– 904.
21Dodge JT, Brown BG, Bolson EL, Dodge HT. Lumen diameter of normal human coronary arteries. Influence of age, sex, anatomic variation, and left ventricular hypertrophy or dilation. Circulation. 1992; 86: 232– 246.